Combustion and Flame 162 (2015) 774–787

Contents lists available at ScienceDirect

Combustion and Flame

journal homepage: www.elsevier.com/locate/combustflame

Autoignition and combustion characteristics of kerosene droplets with dilute concentrations of aluminum nanoparticles at elevated temperatures

Irfan Javed *[,1], Seung Wook Baek *, Khalid Waheed [1]

Division of Aerospace Engineering, School of Mechanical, Aerospace and Systems Engineering, Korea Advanced Institute of Science and Technology (KAIST), 291 Daehak-ro, Yuseong-Gu, Daejeon 305-701, Republic of Korea

ARTICLE INFO

Article history:
Received 25 April 2014
Received in revised form 26 July 2014
Accepted 27 August 2014
Available online 1 October 2014

Keywords:
Droplet combustion
Autoignition
Nanofluid fuels
Nanoparticles
Aluminum
Kerosene

ABSTRACT

In this experimental study, we investigated the effects of high ambient temperatures and dilute concentrations of nanoparticles (NPs) on the autoignition and combustion characteristics of kerosene-based nanofluid droplets. An isolated kerosene droplet containing 0.1%, 0.5% or 1.0% by weight of aluminum (Al) NPs suspended on a silicon carbide (SiC) fiber was suddenly exposed to an elevated temperature (in range 400–800 °C) at atmospheric pressure (0.1 MPa) under normal gravity, and the autoignition and combustion characteristics were examined. The ignition delay time, burning rate constant and combustion characteristics of pure and stabilized kerosene droplets were also observed for comparison. The results indicate that, similar to pure kerosene droplets, the ignition delay time of NP-laden kerosene (*n*-Al/kerosene) droplets also followed the Arrhenius expression and decreased exponentially with increasing temperature. However, the addition of dilute concentrations of Al NPs to kerosene reduced the ignition delay and lowered the minimum ignition temperature to 600 °C, at which pure kerosene droplets of the same initial diameter were not ignited. In contrast to the combustion of pure and stabilized kerosene droplets, the combustion of *n*-Al/kerosene droplets exhibited disruptive behavior characterized by sudden reductions in the droplet diameter without any prior expansions caused by multiple-time bubble formation and their subsequent rupture at or near the droplet's surface. This bubble pop-up resulted in droplet trembling and fragmentation and ultimately led to enhancement in gasification, vapor accumulation and envelope flame disturbance. The NPs were also brought out of the droplets through these disruptions. Consequently, the burning time and total combustion time of the droplets were reduced, and almost no residue remained on the fiber following combustion. Thus, the combustion rate of *n*-Al/kerosene droplets was substantially enhanced compared with pure kerosene droplets at all tested temperatures.

1. Introduction

The volumetric or gravimetric energy contents of metals are considerably higher than the energy densities of traditional liquid fuels. Therefore, in principle, higher combustion energies can be achieved from the combustion of metallized liquid fuels. Because of this fascinating benefit, in the past, many researchers have conducted detailed research on the combustion of such fuels, which are referred to as 'slurry fuels.' Slurry fuels consist of relatively high solid loadings (40–80% by weight) of micron-sized metallic (Al, boron (B), carbon (C) and blend of Al and C) particles in a liquid hydrocarbon carrier. The major drawbacks that limit the practical application of such fuels are incomplete combustion, lower combustion efficiency, unacceptable deposits in the combustion chamber and increased particulate emission in exhaust. The particle agglomeration (which often occurs before and/or during the ignition phase) and longer burning time of the agglomerates are the primary causes of all these side effects [1].

Nanofluid fuels, a new class of nanofluids, are stable suspensions of energetic material NPs in traditional liquid fuels. Nano-powders of energetic materials (*i.e.*, Al, B, C, Fe, and CeO_2) have been used as additives and suspended in conventional liquid fuels in a proper manner that enhances their ignition and

* Corresponding authors. Fax: +82 42 350 3710.
E-mail addresses: ijkasuri@gmail.com (I. Javed), swbaek@kaist.ac.kr (S.W. Baek).
[1] Permanent address: Pakistan Institute of Engineering and Applied Sciences (PIEAS), Nilore 45650, Islamabad, Pakistan.

http://dx.doi.org/10.1016/j.combustflame.2014.08.018
0010-2180/

combustion characteristics. Previous studies have demonstrated significant improvements using such nanofluid fuels including enhanced catalytic effects [2,3], increased ignition probability [4], improved burning rate [5], shortened ignition delay [6] and higher energy release [7]. However, the applications of nanofluid fuels may be limited by the same issues that have made slurry fuels impracticable, such as particle agglomeration and potential emissions of particles. Here, it is important to note that nanofluid fuels are fundamentally different than slurry fuels. Nanofluid fuels are suspensions with relatively low loading rates (~10% by weight) of NPs, such that the physical properties (such as density and boiling point) of base fuels may not significantly change, and nanofluid fuels can be used in existing propulsion and combustion systems with slight modifications. It is expected that due to the addition of nano-scale particles, the size of the agglomerates is reduced. The agglomerates may also be shattered by the microexplosions that occur due to the addition of NPs and that have been previously observed during the evaporation of kerosene-based nanofluid fuel droplets at elevated temperatures [8,9]. These microexplosions occur early in the droplet life time and become more intense with an increase in temperature. Based on the shattering of agglomerates due to such intense microexplosions, it can be anticipated that most of the NPs will be burned during droplet combustion, which reduces particulate emission.

Although our previous research articles [8–10] have been focused on the effects of NP concentrations on the evaporation characteristics of droplets, the present study investigated the effects of NP loading rates on droplet autoignition and overall combustion characteristics. Similar to vaporization [9], the combustion of nanofluid fuel droplet is also a highly complex phenomenon compared with pure liquid fuel droplet combustion because of its multi-component, multi-phase and multi-scale nature. Several physical and chemical processes occur during the combustion of a nanofluid fuel droplet. These processes include mass and energy transport to/between the phases (solid, liquid and gas), evaporation of the liquid fuel, generation of heterogeneous nucleation sites (HNSs) within a droplet, microexplosions (transport of NPs from liquid droplet to flame), combustion of the liquid fuel in vapor phase, vapor accumulation, dynamics of the NPs (*i.e.*, particle diffusions, collisions, aggregation, agglomeration and transported out of droplet), combustion of the solid particles, and their combinations. The interaction of these processes with each other makes achieving a fundamental understanding even more difficult. In addition, the thermophysical properties of nanofluid fuels are significantly different from those of their base fuels. Moreover, these properties can also vary with time because of the continuous change in the concentration of NPs within a droplet. Furthermore, the radiation properties (by absorption) of NPs could also aid in ignition and combustion. Therefore, experimental studies, which are very rare, are required to obtain a basic understanding of the autoignition and combustion behavior of nanofluid fuel droplets.

Sabourin et al. [11] achieved a significant enhancement in the burning rate of monopropellant nitromethane through the addition of 1% (by weight) functionalized graphene sheets into it, which also reduced its ignition temperature. Gan and Qiao [12] observed the burning behavior of ethanol and *n*-decane fuel droplets after loading nano- and micro-sized Al particles into them. Their results revealed that for the same surfactant and particle concentrations, the disruption behavior occurred later and with a much greater intensity in droplets containing micron-sized particles. Later, Gan et al. [13] found a simultaneous combustion of both the droplet and the NPs in dilute suspensions of boron and iron NPs in *n*-decane and ethanol. However, in dense suspensions, most particles were combusted as large agglomerates after the consumption of the liquid fuel. Most recently, we observed [14] an intense disruptive burning behavior of Al NP-laden heptane droplets, which was characterized by multiple expansions and ruptures or 'microexplosions.' Due to these intense and frequent microexplosions, almost no residue from the Al NPs remained on the fiber following combustion, and a separate Al flame was not observed. The overall activation energy obtained for dilute NP concentrations (0.5% by mass) was smaller and that for dense (2.5% and 5.0%) concentrations of NPs larger, than that of pure heptane droplets. It was also anticipated that the addition of dilute concentrations of Al NPs to a low volatile liquid hydrocarbon fuel, where ignition is diffusion limited, might reduce the ignition delay time and might also lower the ignition temperature.

In our previous work [14], we used a highly volatile, single-component liquid hydrocarbon (heptane) as a base fuel. In the present study, we used kerosene, which is a multi-component liquid hydrocarbon and a blend of relatively nonvolatile petroleum fractions. Kerosene was selected because most aviation fuels (*e.g.*, JP-5, JP-7, JP-8, or Jet A/A-1) and liquid hydrocarbon propellants (*e.g.*, RP-1) can be described generically as kerosene [15]. The autoignition and combustion characteristics of NP-laden kerosene droplets will provide us with an improved understanding of the effects of adding NPs to such multi-component hydrocarbon fuels. Other reports [12,13] describe the simple qualitative behavior of the combustion of nanofluid fuel droplets where the droplets were ignited by a heated wire. Therefore, these reports were not able to include the effects of NPs on autoignition delay times or the droplet combustion behavior at various elevated temperatures. In addition, they could not explain the effects of NPs on combustion rate constants. To the best of our knowledge, no study has been reported regarding the effects of the addition of various concentrations of NPs on autoignition and the combustion characteristics of kerosene-based nanofluid fuel droplets at elevated temperatures.

Motivated by the above, the autoignition and combustion characteristics of kerosene-based nanofluid fuel droplets with dilute concentrations of Al NPs were investigated in this paper. The effects of particle-loading rate on droplet ignition and burning behavior were examined. The distinguishing features presented in nanofluid droplet combustion were identified through a comparative analysis with pure and stabilized fuel droplet combustion. Moreover, the key phenomenon of particle escape from the nanofluid fuel droplet is discussed in comparison to previous studies [12,14].

2. Experimental method

The materials and instruments used for current research work were the same as already described in previous articles [8,9]. All these materials were used in their original form as received from suppliers except the Al NPs, whose surfaces were modified before dispersing them into kerosene.

The preparation of stable, kerosene-based nanofluid fuels was also elaborated in detail previously [8,9]. Briefly, the purchased NPs were coated with oleic acid (OA) in a planetary ball mill, which improves their dispersion stability in liquid hydrocarbons. These Al/OA pastes were mixed in different proportions with kerosene, and 0.1%, 0.5% and 1.0% Al NP-laden kerosene (*n*-Al/kerosene) suspensions were obtained. In this case and for the remainder of this paper, mass percentage values are used.

The experimental apparatus used in the current research work was designed, fabricated and installed by our group in the past and is discussed in detail in previous studies [16–19]. The same experimental setup was also employed in our previous studies regarding the evaporation characteristics of nanofluid fuel droplets [8–10]. The experimental procedure was described in detail in those research articles [8–10] along with data reduction and analysis, experimental errors and reproducibility of the results. Briefly,

an isolated *n*-Al/kerosene droplet was suspended by a 100-μm diameter SiC fiber. The heat loss from the fiber can be neglected during most of the droplet's lifetime for fiber diameters of less than 100 μm [20]. The fiber effects are not problematic in present study; because of the systematic comparison with the experiments using pure kerosene fuel as a reference case in which similar supporting fiber was also used. The initial average diameter of a droplet was 1.0 ± 0.1 mm. Dry air was used as an oxidizer for combustion, and the ambient pressure was kept constant at 0.1 MPa. High-temperature ambience was provided by an electric furnace which rises the temperature from room temperature to 98% of the set value in less than 50 ms for the low ambient pressure (less than 1.0 MPa) tests [18]. The electric furnace is capable to maintain the ambient temperature of the droplet to nearly a constant value without significant variation. An amount of air at room temperature inevitably flows into high temperature furnace during its fall resulted a little fluctuation in furnace inner temperature, especially in early lifetime of the droplet. The bandwidth of this fluctuation becomes a little wider as the set value of furnace temperature is increases due to a larger temperature difference between the furnace inside and fresh air. Note that the ceramic shields cover the heating element coils placed at furnace inner walls, so that the radiative heat transfer from coils to droplet is also minimized. The ambient temperature was varied in the range 400–800 °C, which was higher than the autoignition temperature of kerosene (295 °C) as well as both below and above the melting point of Al NPs (660 °C). The Al NPs are passivated by an oxide layer of Al_2O_3 of thickness of few nanometers. This oxide layer is sufficiently thermally resistant to prevent ignition of the NPs. However, in present study, the Al NP surfaces were modified by a method, producing oxide-free, ligand-protected NPs [3]. The combustion process was recorded using a high-speed charge-coupled device (CCD) camera. For each experimental condition, tests were conducted at least three times to ensure the reproducibility and consistency of the results, and the most frequent values are chosen to display. The captured images were analyzed using a flexible image processing code to extract the droplet diameter as discussed in previous study [10]. The temporal variation of the droplet diameter was obtained during the whole combustion process. If the droplet combustion follows the d^2-law, then the combustion rate can be expressed as the time derivative of the droplet diameter squared, $K_c = -d(d^2)/dt$ [21,22]. In that case, the droplet combustion rate was obtained from the temporal history of the droplet diameter squared by measuring the slope of its linear regression.

3. Results and discussion

3.1. Droplet autoignition

In this section, we describe the effects of the addition of dilute concentrations of NP on the autoignition characteristics of multicomponent hydrocarbon fuel (kerosene) droplets at various elevated temperatures. The effects of the addition of NPs were distinguished by comparing the autoignition of nanofluid droplets with pure and stabilized fuel droplets. A similar procedure as that used to study the autoignition delay times for the heptane-based nanofluid fuel droplets [14] was adopted in this investigation. The ignition delay time was defined as the time from the entry of the droplet into the furnace to the ignition radiation [23]. The occurrence of ignition was identified visually by the appearance of a flame through the use of high-speed color photography [18]. The experimental apparatus used here is based on a non-premixed configuration, and so the autoignition delay time described here is the total ignition delay time (a summation of physical delay and chemical delay).

3.1.1. Autoignition of a pure fuel droplet

Figure 1 shows a comparison of the ignition delay times of kerosene droplets between a previous study by Khan et al. [18] and the present study. In this figure, the logarithmic ignition delay time is plotted on the ordinate, and the inverse of absolute ambient temperature is shown on the abscissa. At atmospheric pressure, an increase in temperature reduces the ignition delay times as reported previously [18]. The comparison indicates that a linear relationship between τ and $1000/T$ (or an Arrhenius expression, $\tau = A\exp(D/T)$) can be considered for the ignition delay data of the kerosene droplets obtained in present work, as reported in a previous work by our group [18]. However, the present ignition delay times of the kerosene droplets were lower than the values obtained previously probably because of the difference in droplet initial diameters and fiber diameters that were used for droplet suspensions. Khan et al. [18] suspended the droplets with initial diameters in the range of 1.0–1.2 mm on quartz fibers with diameters of 0.125 and 0.2 mm that were rounded at the tips with bead diameters of 0.25 and 0.35 mm, respectively. However, in our current research, each droplet was suspended on a 0.1-mm SiC fiber with no bead at its tip, and droplets having similar initial diameters ranging from 0.904 to 1.033 mm were selected from the experimental data to minimize the effect of the initial droplet size on ignition delays. Moreover, kerosene being a multicomponent fuel, cannot be represented by one of its constituent components solely. Indeed, its ignition delay time is affected by the boiling point, volatility (physical delay) and chemical reactivity (chemical delay) of its constituent components (paraffins, naphthenes and aromatics).

3.1.2. Autoignition of a stabilized fuel droplet

Autoignition delay times of stabilized kerosene (OA/kerosene) droplets were measured to understand the effect of the addition of OA on autoignition characteristics. These ignition delays of the stabilized kerosene droplets provide another baseline to distinguish the effect of the addition of NPs on droplet autoignition behavior.

Figure 2 shows the ignition delay of stabilized kerosene droplets containing 0.25% and 0.50% OA. The figure shows that the effect of OA is relatively weak. It is shown later that the effect of Al-NP addition to kerosene is much more pronounced. It has been already well established that the ignition behavior of a bi- or multicomponent fuel spray is controlled by its high volatility components and

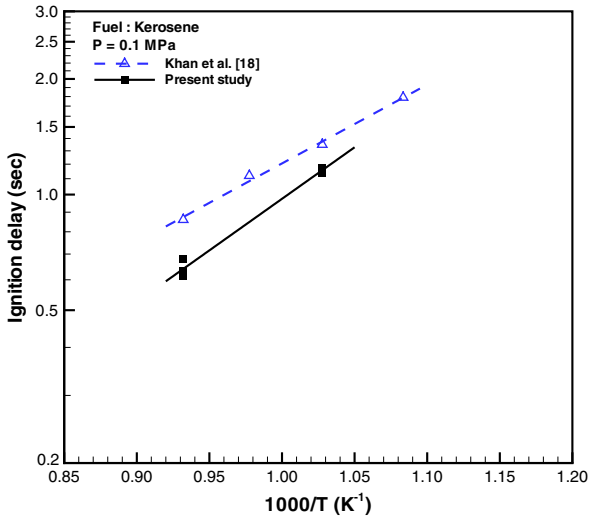

Fig. 1. Comparison of ignition delay times of kerosene droplets between the present study and previous data by Khan et al. [18] at various ambient temperatures.

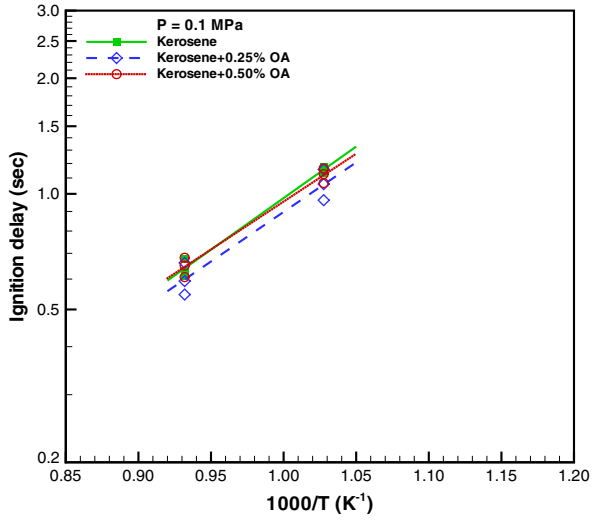

Fig. 2. Ignition delay times of stabilized kerosene droplets with dilute concentrations (0.25% and 0.50%) of oleic acid (OA).

hardly affected by the significant amount of its low volatility components. This was concluded by Aggarwal [24] based on both numerical and experimental investigations. An important implication here is that the ignitability of kerosene droplets (boiling point 180–220 °C) is hardly affected by the addition of a low amount of OA (boiling point 360 °C).

3.1.3. Autoignition of n-Al/kerosene droplets

3.1.3.1. Droplet behavior prior to autoignition. Figure 3 shows the temporal variation of the normalized diameter squared of the kerosene and *n*-Al/kerosene droplets with Al NP loadings of 0.1%, 0.5%, and 1.0% up to ignition and at various ambient temperatures. Figure 3a shows these data at relatively low temperatures (400, and 500 °C), whereas Fig. 3b presents the data at relatively higher temperatures (600, 700 and 800 °C) on their corresponding colored[2] *x*-axes. The initial heating-up period of the *n*-Al/kerosene droplets was shorter than that of the pure kerosene droplets at all temperatures, regardless of NP loadings. This effect is more prominent at relatively low temperatures in the range 400–600 °C. The successive vaporization period of the *n*-Al/kerosene droplets was also reduced because of the increased evaporation rate. This fact is more significant at relatively higher temperatures (600–800 °C). Consequently, the ignition delay time of the *n*-Al/kerosene droplets was shortened compared with pure kerosene droplets. The most significant effect of NPs addition to kerosene is the appearance of ignition at 600 °C. It is important to note that pure kerosene droplets with a 1-mm initial diameter were ignited only at 700 and 800 °C under atmospheric pressure, whereas the *n*-Al/kerosene droplets of the same initial diameters were also ignited at a lower temperature, 600 °C.

To understand the mechanism responsible for this, it is necessary to investigate the vaporization behavior of the droplets before ignition at 600 °C. The pure and *n*-Al/kerosene droplets exhibited an initial heating-up period and then followed the d^2-law vaporization. However, with the addition of 0.1% NPs, the initial heating-up time decreased slightly, which was further reduced by increasing Al NP loading to 0.5% and 1.0%. The vaporization behavior of the 1.0% Al NP suspension droplets was slightly different. Compared with the 0.5% suspension, the droplets containing 1.0% Al NPs evaporated faster initially and then slightly slower during the later

[2] For interpretation of color in Fig. 3, the reader is referred to the web version of this article.

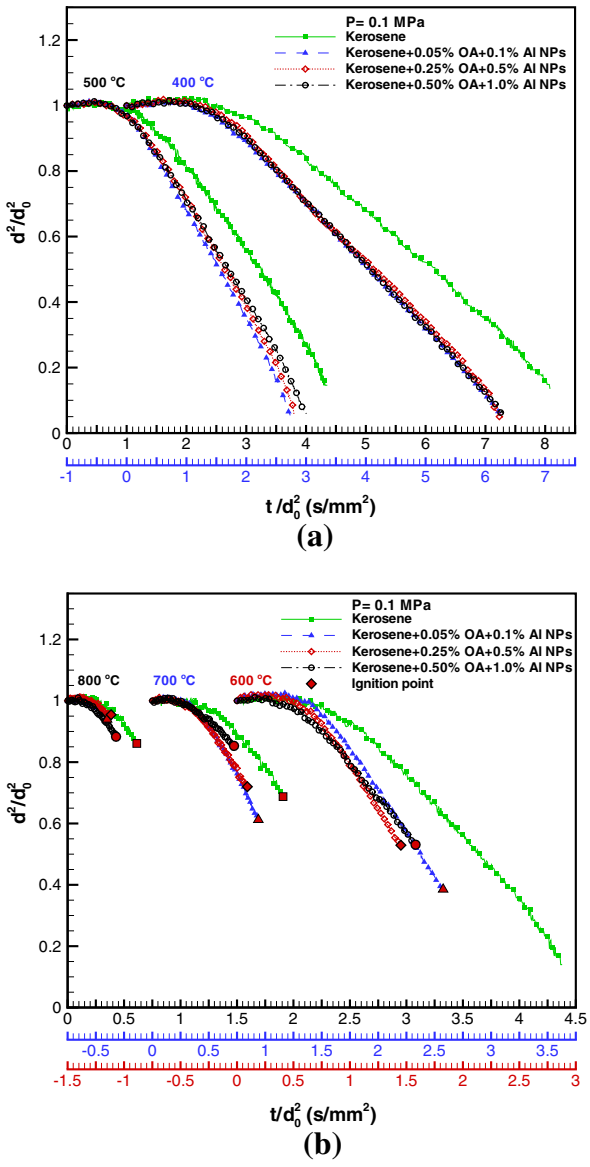

Fig. 3. Normalized temporal histories of kerosene and *n*-Al/kerosene droplets' diameters squared, for droplets containing 0.1%, 0.5% and 1.0% Al NP concentrations, until their ignition.

stages of evaporation; due to this slight reduction, the vaporization period was longer than that of the 0.5% suspension droplets. This was likely caused by the formation of NP agglomerates in the 1.0% Al NP suspension droplets, as discussed previously [19]. The vaporization rate was calculated by applying least squares regression to the linear vaporization period prior to ignition. Figure 4 shows a comparison of pre-ignition vaporization rate of pure and *n*-Al/kerosene droplets at 400–600 °C. At 600 °C, the addition of 0.1%, 0.5% and 1.0% Al NPs to kerosene droplets enhanced the vaporization rate to 35.5%, 51.3% and 14.7%, respectively, compared with pure kerosene droplets. The smaller enhancements in the evaporation rate of 1.0% Al NP suspension droplets compared with the 0.1% and 0.5% Al NP suspension droplets was likely due to the formation of NP agglomerates in those suspension droplets. Such substantial enhancement in the evaporation rate of *n*-Al/kerosene droplets was already reported in our previous study [19].

The autoignition temperature of bulk kerosene fuel is approximately 295 °C, but a single droplet (1 mm initial diameter) of kerosene fuel was not ignited at even 600 °C under atmospheric pressure (as also reported in previous study by Khan et al. [18]).

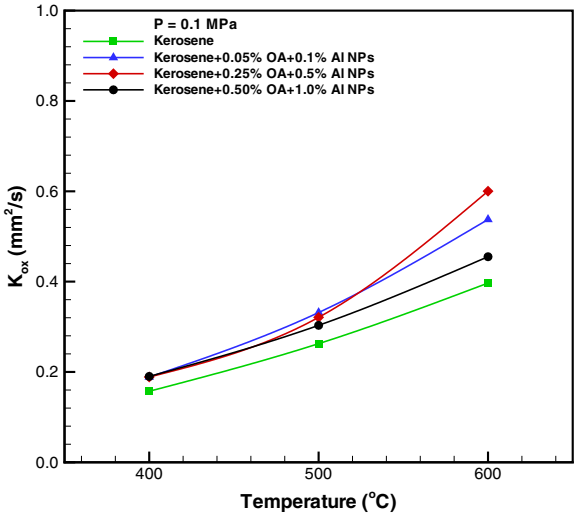

Fig. 4. Comparison of pre-ignition vaporization rate of pure kerosene and *n*-Al/kerosene droplets with dilute concentrations (0.1%, 0.5% and 1.0%) of Al NPs.

This is because of its low evaporation rate at this temperature, which is not able to produce enough vapors that can mix with the air in the proportions required for initiation of ignition and subsequent combustion. However, the addition of Al NPs to kerosene droplets first led to a slight decrease in the initial heating-up period probably due to increased thermal diffusivity [6]. Then, the presence of the OA-coated NPs enhanced the pre-ignition vaporization rate of kerosene droplet substantially and produced such amount of vapors that was enough to initiate the ignition. It implies that the addition of Al NPs to a low volatility liquid hydrocarbon fuel reduces the ignition delay time through enhancement in vaporization rate and also results in a decrease in ignition temperature. Probably, the enhanced thermal diffusion as a result of NPs addition to fuel droplet caused these effects in NP-laden kerosene droplets.

3.1.3.2. Effect of ambient temperature on the autoignition delay time. Figure 5 shows a comparison of the ignition delay times of *n*-Al/kerosene droplets containing 0.1%, 0.5% and 1.0% Al NPs with pure kerosene droplets at various elevated temperatures. To understand the effects of the ambient temperature, the logarithm

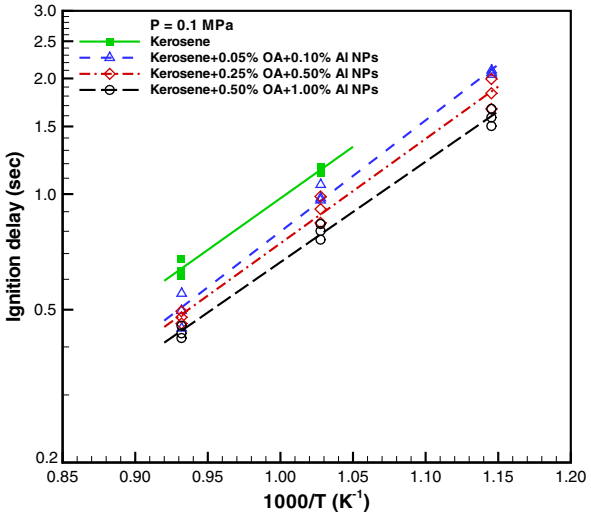

Fig. 5. Ignition delay times of *n*-Al/kerosene droplets with dilute concentrations (0.1%, 0.5% and 1.0%) of Al NPs.

Table 1
Constant values for pure kerosene and *n*-Al/kerosene droplets calculated from experimental data of current study correlated by empirical equation of ignition delay, $\tau = A\exp(D/T)$.

Fuel	Initial diameter range, d_0 (mm)	Temperature range, T (K)	A (ms)	D (K)
Kerosene	0.904–1.033	973–1073	2.02	6181
Kerosene + 0.05% OA + 0.1% Al NPs	0.978–1.028	873–1073	1.05	6640
Kerosene + 0.25% OA + 0.5% Al NPs	0.933–1.057	873–1073	1.42	6262
Kerosene + 0.50% OA + 1.0% Al NPs	0.900–1.070	873–1073	1.62	6016

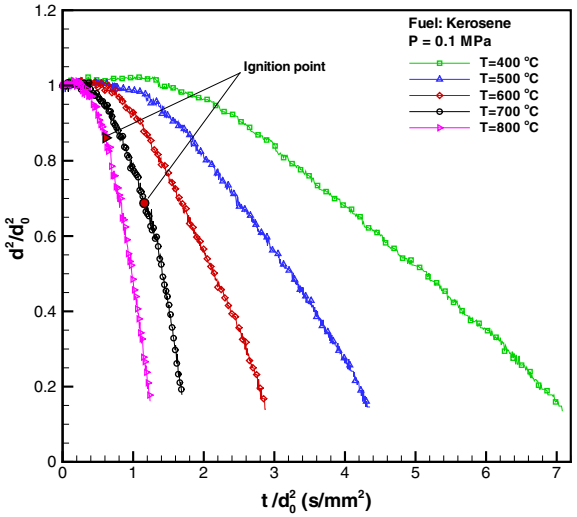

Fig. 6. Temporal variations of normalized diameter squared of pure kerosene droplets combustion conducted at various ambient temperatures.

of the ignition delay times of pure and nanofluid droplets were plotted as a function of the inverse ambient temperature, as shown in Fig. 5. The ignition delay data of kerosene-based nanofluid droplets containing dilute concentrations of Al NPs display a similar trend to pure kerosene droplets, as expressed by the Arrhenius functional form, $\tau = A\exp(D/T)$, which decreased exponentially with increasing temperature. However, the ignition delay times of *n*-Al/kerosene droplets were lower than those of pure kerosene droplets at these temperatures. The values of the constants A and D for pure kerosene and *n*-Al/kerosene droplets were calculated from our experimental autoignition delay data and are listed in Table 1. The constants for NP-laden kerosene droplets reported here depend upon the Al NP loading in the droplet. With 0.1% and 0.5% suspension droplets, larger values of D and smaller values of A were obtained in comparison with pure kerosene. However, with the 1.0% NP suspension, a smaller value of D was obtained, as listed in Table 1.

3.1.3.3. Effect of NP concentration on the autoignition delay time. The ignition delays of *n*-Al/kerosene droplets containing dilute concentrations of Al NPs are considerably affected by the concentrations of NPs. As the concentration of NPs increased from 0.1% to 1.0%, the ignition delay times were reduced monotonically at all tested temperatures in the range 600–800 °C. The 1.0% NP suspension droplets demonstrated the maximum decrease in ignition delay time.

Kerosene is a multicomponent liquid hydrocarbon fuel, which has a substantially lower volatility than *n*-heptane. Because of its high boiling range (180–270 °C) and multicomponent nature,

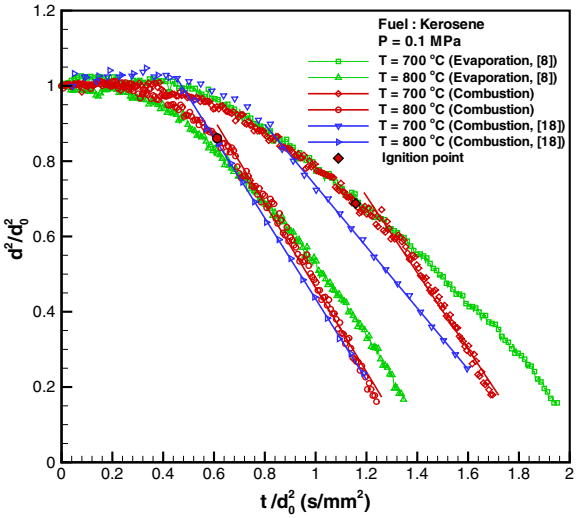

Fig. 7. Comparison of normalized combustion histories along with least squares fit for linear combustion portion conducted out at 700 and 800 °C between the present study and a previous study by Khan et al. [18], as well as with previously reported corresponding evaporation histories [8].

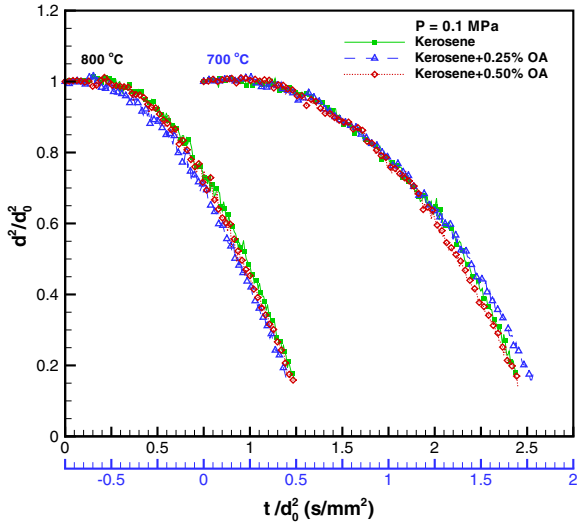

Fig. 9. Temporal variations of diameter squared of burning stabilized kerosene droplets with dilute concentrations (0.25% and 0.50%) of OA.

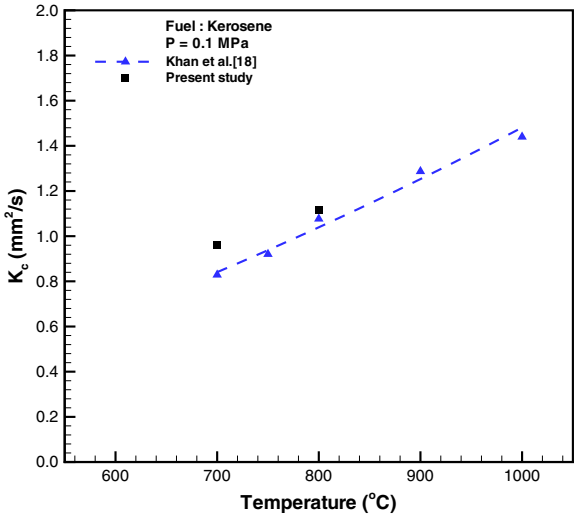

Fig. 8. Comparison of combustion rate constants of pure kerosene droplets between present study and a previous study by Khan et al. [18] under various ambient temperatures.

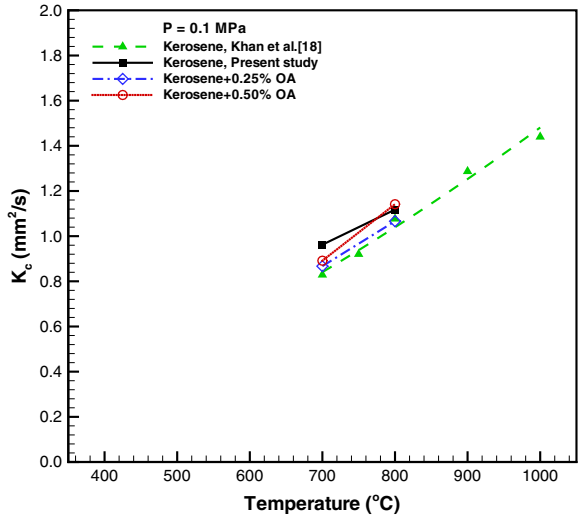

Fig. 10. Comparison of combustion rate constants between pure kerosene and stabilized kerosene droplets containing 0.25% and 0.50% OA at elevated temperatures.

kerosene displays a significant physical delay (initial heating-up time and pre-ignition vaporization period) compared with pure *n*-heptane droplets studied previously [14]. The addition of dilute concentrations of Al NPs decreased these heating-up and vaporization periods of kerosene droplets, which decreased their physical delays and, overall, lowered their ignition delay times. This fact is clearly identified in the temporal vaporization history prior to ignition of *n*-Al/kerosene droplets containing dilute concentrations of Al NPs (Fig. 3b). These results imply that the addition of dilute concentrations of Al NPs lowered the minimum ignition temperature and reduced the ignition delay times of kerosene droplets by decreasing their physical delays.

3.2. Droplet combustion

In this section, we discuss the effects of the addition of various concentrations of Al NPs on the droplet combustion at high ambient temperatures. The combustion rate constant and burning behavior of pure and stabilized kerosene droplets was investigated as a baseline for comparison. This helped us to distinguish the effects of the addition of the Al NPs on the combustion behavior of the kerosene-based nanofluid fuel droplets. The temperature was varied in the range 400–800 °C, and the pressure was maintained at 0.1 MPa.

3.2.1. Combustion of pure fuel droplets

Figure 6 shows the variation in the normalized diameter squared with the normalized time for pure kerosene droplets in a temperature range of 400–800 °C. The ignition and subsequent combustion of pure kerosene droplets only occurred at 700 and 800 °C. After ignition, the variation in droplet diameter squared became approximately linear with time, such that the combustion of pure kerosene droplets followed the d^2-law. Here, it is important to mention that due to the high boiling point (180–270 °C) of kerosene compared with the boiling temperature of *n*-heptane

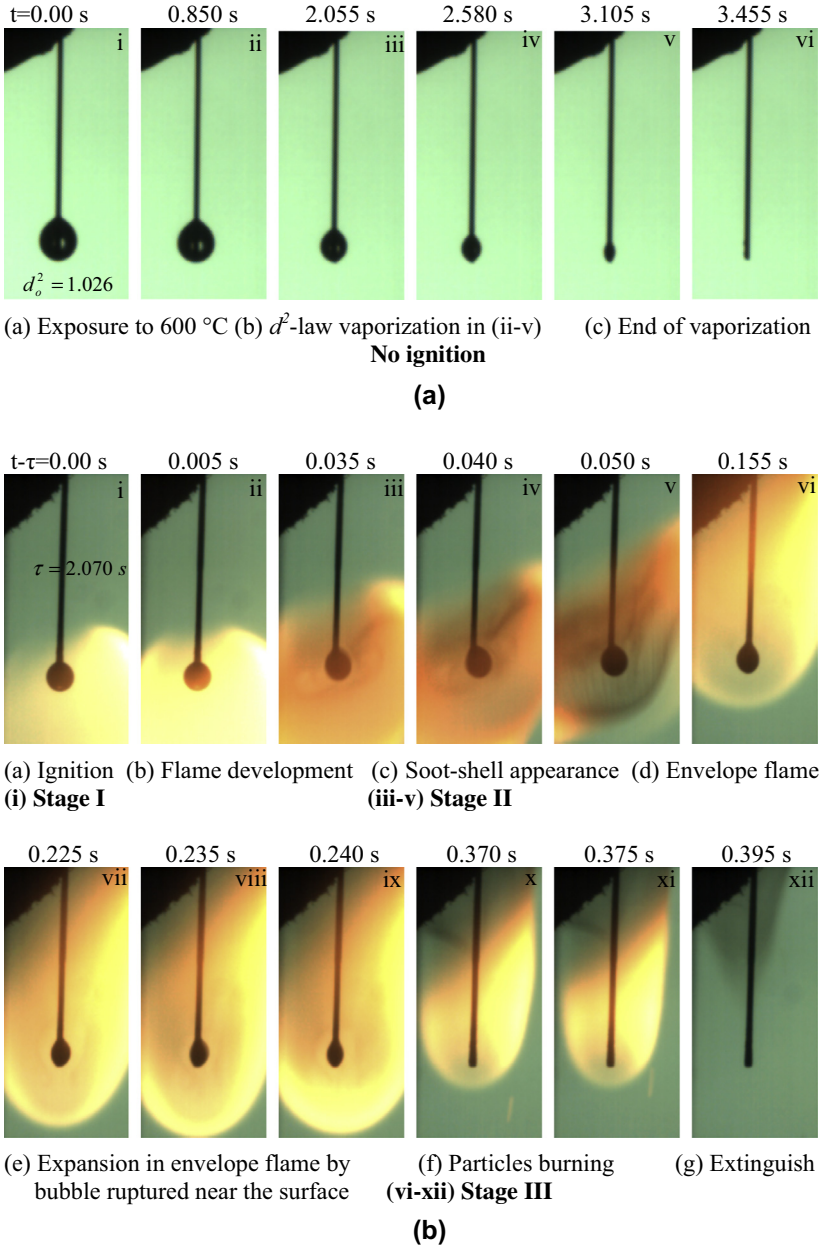

Fig. 11. Successive pictures of burning droplets starting from their ignition till the flame extinguish at 600 °C (a) pure kerosene, (b) kerosene + 0.05% OA + 0.1% Al NPs, (c) kerosene + 0.25% OA + 0.5% Al NPs and (d) kerosene + 0.5% OA + 1.0% Al NPs.

(98 °C), the fiber effects disappeared during the combustion of pure kerosene fuel droplets. During the combustion of pure *n*-heptane droplets, an expansion in droplet diameter was observed slightly after ignition [14], which was likely caused by the fiber.

Figure 7 shows a comparison of the droplet burning histories along with a least squares fit of the linear combustion portion at 700 and 800 °C between the present study and a previous study by Khan et al. [18], in addition to showing the comparison with previously reported corresponding evaporation histories [8]. The figure clearly indicates that after an initial heating-up period, the droplet follows the d^2-law in both cases, either evaporation or combustion [20]. However, with combustion, after ignition, the droplet diameter history departed from the corresponding evaporation case through a rapid reduction in diameter, which resulted in high burning rate. This is due to the appearance of flame around the droplet, which resulted in more and faster heat transfer to the droplet. The droplet-burning rate constant (K_c) was calculated from the slope of the linear part of the droplet diameter curve after the ignition point. The difference in combustion histories and their corresponding linear curves was due to the difference in the initial diameters of droplets, which were suspended on fibers in both studies as described previously in Section 3.1.1. The combustion rate constants calculated by the least squares fits (in Fig. 7) were compared in Fig. 8. The present value of the combustion rate constant was matched well to that previously obtained value at 800 °C. However, at 700 °C, the present combustion rate constant is slightly higher than previously achieved value.

3.2.2. Combustion of stabilized fuel droplets

To understand the combustion behavior of kerosene-based nanofluid fuel droplets at elevated temperatures, it is essential to study the combustion characteristics of stabilized kerosene droplets with the addition of various concentrations of OA while holding the temperature constant. The combustion rates of the

stabilized kerosene droplets provide another baseline to distinguish the effect of the addition of NPs on droplet combustion behavior.

Figure 9 shows the normalized temporal histories of the diameter squared of kerosene droplets with 0.25% and 0.5% surfactant (OA) at various ambient temperatures (700–800 °C). Similar to pure kerosene droplets, the ignition and combustion of stabilized kerosene droplets occurred only at these temperatures. The general combustion behavior of stabilized kerosene droplets was similar to that of pure kerosene droplets, *i.e.*, after a finite heating-up period, the droplet vaporized, ignited and its diameter squared decreased linearly and followed the d^2-law. The combustion rate constants of stabilized kerosene droplets were calculated by using the least squares method in the linear combustion part.

Figure 10 compares the combustion rate constants of stabilized kerosene droplets containing 0.25% and 0.5% OA with pure kerosene droplets at 700–800 °C. The burning rate of stabilized kerosene droplets was almost equal or slightly lower than the combustion rate of pure kerosene droplets at these temperatures. Because only low concentrations of OA (surfactant) were added in the kerosene, the combustion rate of stabilized kerosene droplets was little affected and remained almost the same as that of pure kerosene droplets at these temperatures.

3.2.3. Combustion of n-Al/kerosene droplets

3.2.3.1. General combustion behavior. The combustion of isolated *n*-Al/kerosene droplets was investigated at temperatures in the range 400–800 °C and at atmospheric pressure. Prior to a comparative analysis and discussion regarding the combustion of the *n*-Al/kerosene droplets, it is useful to review the literature related to the burning behavior of nanofluid fuels droplets. Gan and Qiao [12] identified five distinct stages, *i.e.*, preheating and ignition, classical combustion, microexplosions, surfactant flame, and Al droplet flame, in Al NPs laden *n*-decane and ethanol fuel droplet combustion. During the combustion of *n*-Al/heptane [14], we observed four distinct regimes *i.e.*, ignition, vapor accumulation, microexplosion and surfactant flame. Classical combustion and the Al droplet flame or Al agglomerate combustion reported in a previous study [12] were not detected during the combustion of heptane-based nanofluid droplets. The *n*-Al/heptane droplets underwent a larger

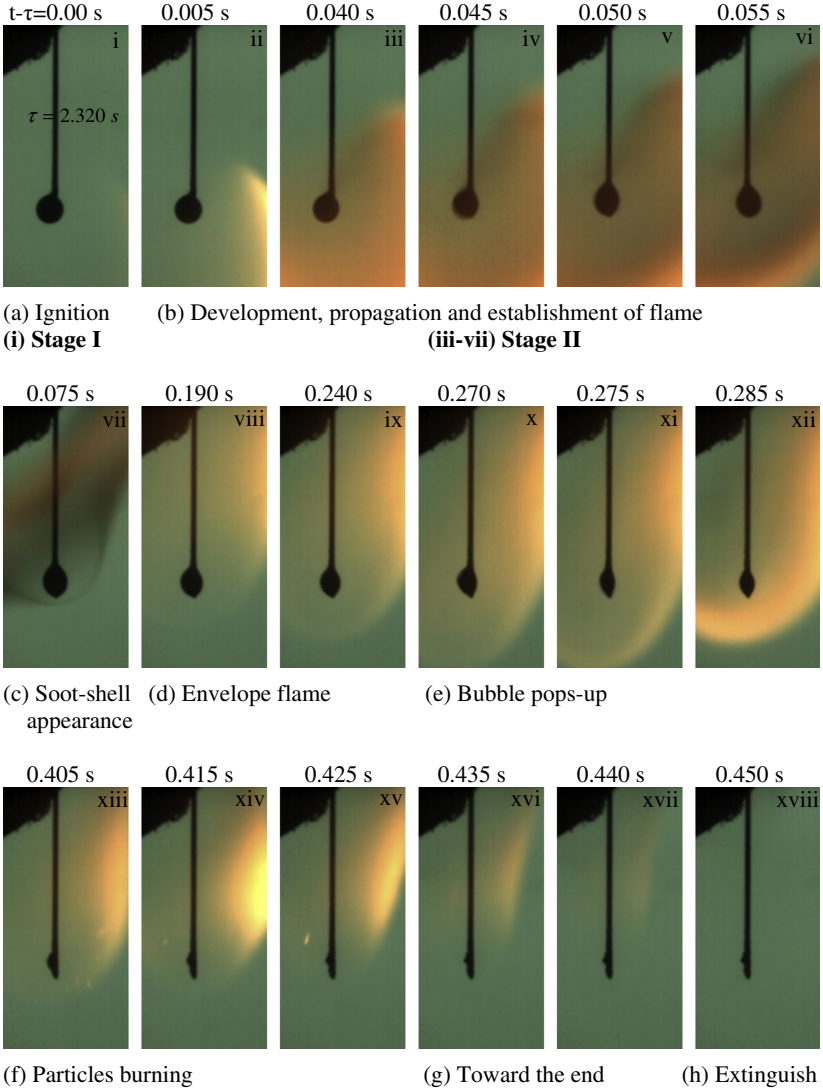

Fig. 11 (*continued*)

expansion and subsequent contraction, with smaller droplets being ejected from the primary droplets, even prior to ignition. The droplet exhibited disruption (*i.e.*, swelling and contraction) behavior again, and this process (known as microexplosion) was repeated several times until the droplet diameter was reduced significantly. These intense microexplosions caused nearly all of the NPs to move out of the droplet and to burn in a primary or secondary (surfactant) flame. Therefore, almost no agglomerates (*i.e.*, residue) remained on the fiber and an 'Al droplet flame' was not observed in *n*-Al/heptane droplet combustion [14].

Figures 11 and 12 show sequential images which describe the combustion of pure kerosene and *n*-Al/kerosene droplets at 600 and 800 °C. These images of the burning droplets are shown to highlight the investigated effects of elevated temperature on the combustion characteristics of nanofluid droplets. Subfigures a–d correspond to pure kerosene and 0.1%, 0.5%, and 1.0% *n*-Al/kerosene droplets, respectively. Figure 13 shows the temporal variation of the normalized diameter squared of the pure kerosene droplets, as well as *n*-Al/kerosene droplets containing 0.1%, 0.5%, and 1.0% Al NPs whose surfaces were coated with 0.05%, 0.25%, and 0.50% of OA, respectively, at various combustion temperatures (600, 700 and 800 °C). A simultaneous side-by-side visualization of the data in these figures is shown in Supplementary video.

Figures 11a and 12a show the combustion behavior of pure kerosene droplets at 600 and 800 °C, respectively. On exposure to 600 °C, the pure kerosene droplet vaporized, following the d^2-law until the end, and was not ignited at this temperature. However, at 800 °C, the pure kerosene droplets were ignited and exhibited three main stages: ignition, vapor accumulation, and d^2-law combustion (*i.e.*, classical droplet combustion), similar to heptane (a single-component hydrocarbon fuel) droplet combustion [14]. During the development of the flame, a soot-shell appeared for a very short duration (0.015 s), which is a commonly observed characteristic of kerosene droplet combustion at elevated pressures [18]. Following this, a bright yellow, luminous envelope flame was established, which was maintained for the majority of the lifetime of the droplet combustion.

Regardless of the concentration of the Al NPs, the combustion of the *n*-Al/kerosene droplets was mainly composed of three regimes: ignition, vapor accumulation, and combustion with fragmentation.

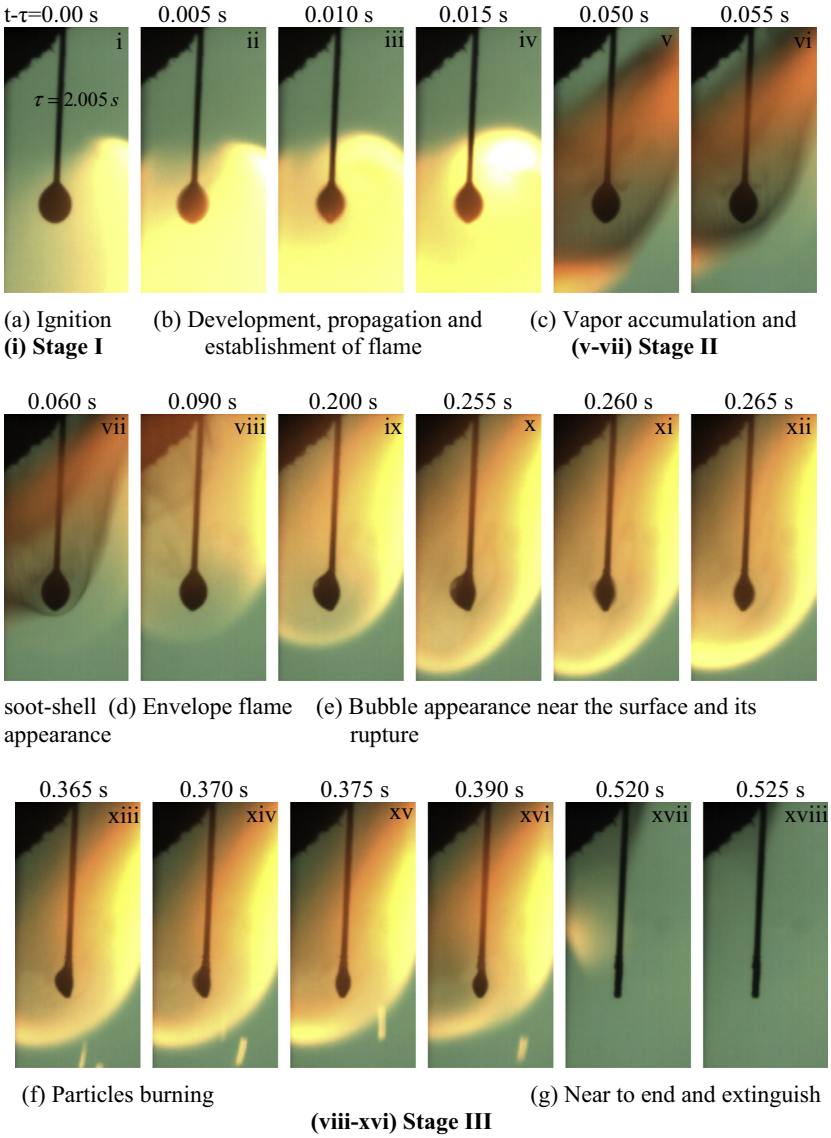

Fig. 11 (*continued*)

The first significant difference of the *n*-Al/kerosene droplets combustion with pure kerosene droplet was the increased vapor accumulation lasted much longer in droplet's lifetime after the ignition. Shortly following ignition, the kerosene droplets containing NPs underwent a sudden reduction in their diameters due to bubble nucleation at the droplet's surface and its subsequent rupture, as shown by the images labelled stage II in Figs. 11b–d and 12b–d. The sudden reduction in droplets diameters after the ignition point is more prominent in Fig. 13. During the bubble rupture, a few smaller droplets, along with NPs and/or aggregates of NPs, were ejected from the surface of primary droplet. The emitted fragments were significantly smaller than the primary droplet and burned along with the ejected NPs. This disruptive process occurred during the development, propagation and establishment of flame and enhanced the gasification of the liquid fuel significantly compared with the pure kerosene droplets. This resulted in greater vapor accumulation and soot-shell appearance than the combustion of the pure kerosene droplets. The phenomena of vapor accumulation (stage II) is more pronounced at relatively higher temperature (800 °C), where it lasted much longer as shown in the snapshots labelled stage II in Fig. 12b–d. At the end of stage II, an envelope flame was established around the droplet. The droplet exhibited disruption (*i.e.*, formation and rupture of bubble at the surface of droplet) behavior again, which expanded (disturbed) the envelope flame, and this process was repeated several times until the droplet diameter was reduced significantly, as shown in the snapshots labelled stage III in Figs. 11b–d and 12b–d. Almost all NPs combusted during this process, and nearly all of the liquid fuel

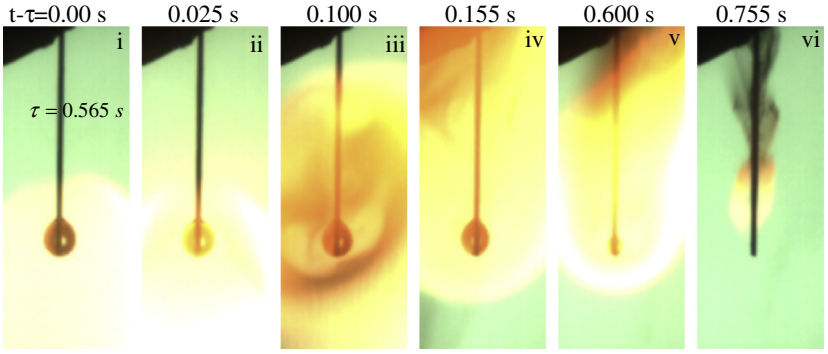

(a) Ignition (b) Flame development (c) Soot (d) Steady burning (e) Near to end

(i) Stage I **(iii) Stage II** **(iv-vi) Stage III**

(a)

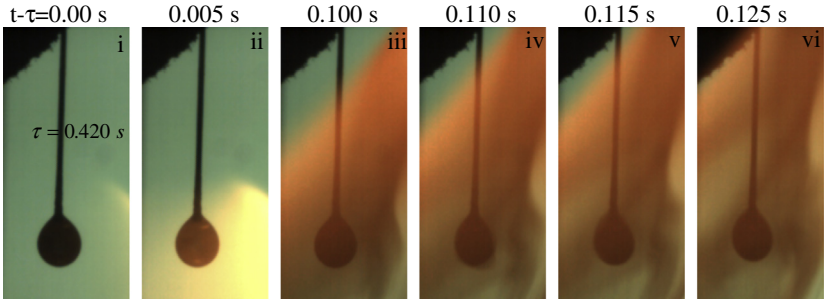

(a) Ignition (b) Flame development (c) Vapor accumulation and bubbles pops up near the droplet's surface

(i) Stage I **(iii-vii) Stage II**

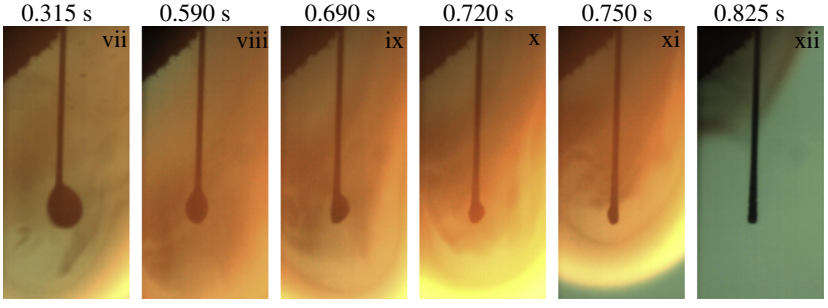

(d) Disruptive burning (e) Particles combustion (f) Extinguish

(viii-xii) Stage III

(b)

Fig. 12. Successive pictures of burning droplets starting from their ignition till the flame extinguish at 800 °C (a) pure kerosene, (b) kerosene + 0.05% OA + 0.1% Al NPs, (c) kerosene + 0.25% OA + 0.5% Al NPs and (d) kerosene + 0.5% OA + 1.0% Al NPs.

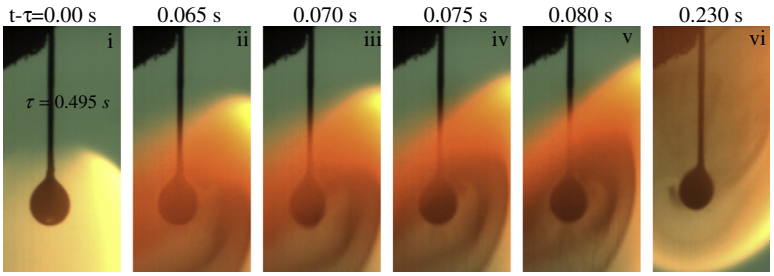

(a) Ignition (b) Development, propagation and establishment of flame along with soot generation

(i) Stage I

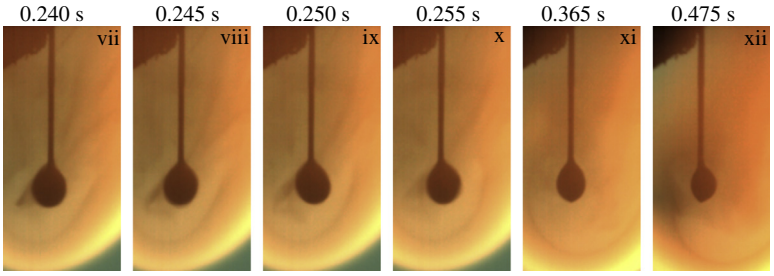

(c) Bubbles pop up near the surface (d) Envelope flame

(ii-x) Stage II

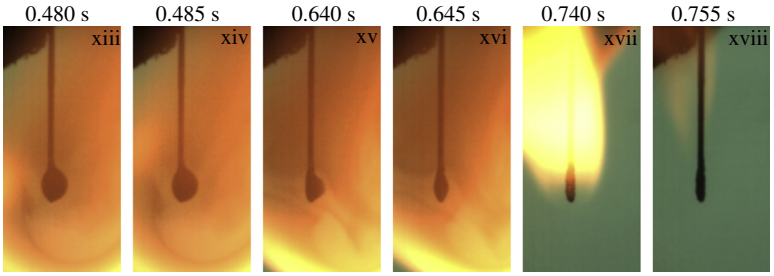

(e) Disruptive combustion (f) Particles burning (g) Near to end

(xi-xviii) Stage III

(c)

Fig. 12 (*continued*)

was consumed; the envelope flame became weaker and was extinguished. Following the extinction of flame, almost no agglomerates remained at the tip of the fiber.

The other distinguishing feature of the addition of Al NPs to kerosene droplets was the onset of bubble formation and their rupture, which caused a sudden reduction in the droplet's diameter during combustion, as seen in Fig. 13. Due to this disruptive behavior, the combustion of *n*-Al/kerosene droplets did not follow the classical d^2-law. Regardless of the Al NP concentration, the sudden reductions in droplets' diameters (due to bubble formation and their subsequent ruptures) were observed at all combustion temperatures (600–800 °C). These disruptions transported the NPs out of the droplets and reduced the burning time and total combustion time of *n*-Al/kerosene droplets compared with pure kerosene droplets. It is noteworthy that this irregular behavior was not observed during the combustion process of pure or stabilized kerosene droplets. However, such disruptions were previously observed in the evaporation process of kerosene-based nanofluid droplets as discussed in Ref. [19]. Here, it is also important to mention that the droplet fragmentation without any prior droplet expansion is different than 'microexplosion', which is the repeated expansion and subsequent rupture of the droplet observed previously in Refs [9,14]. The abrupt reduction in droplet diameter was likely due to the sudden escape of vapors from the droplet surface. As the nanofluid fuel droplets were autoignited and a flame appeared around the droplets, the Al NPs present at or just inside the droplets' surface were heated by the flame (or absorbed the flame radiation) and may have attained a temperature higher than the local boiling point of the liquid fuel. These Al NPs provided multiple heterogeneous nucleation sites (HNSs) for the surrounding liquid that generated superheated vapors. These superheated vapors may have been the cause of droplets' fragmentation during the nanofluid droplets' combustion. In the case of the dilute concentrations of Al NPs, the added Al NPs were not enough to form a shell at the droplet surface that could raise its surface temperature. They only provided HNSs at or near to the droplet surface [19].

In overall, during the combustion of the *n*-Al/kerosene droplets, some stages were found similar to the regimes observed during the combustion of *n*-Al/heptane droplets (*i.e.*, vapor accumulation and disruptive combustion deviate from d^2-law). However, the other stage of surfactant flame was absent. Possibly due to the reduced difference between the boiling points of kerosene and OA and the multicomponent nature of kerosene, a separate surfactant flame was not observed as observed previously in *n*-Al/heptane droplets [14]. Vapor accumulation or a sooty flame is characteristic

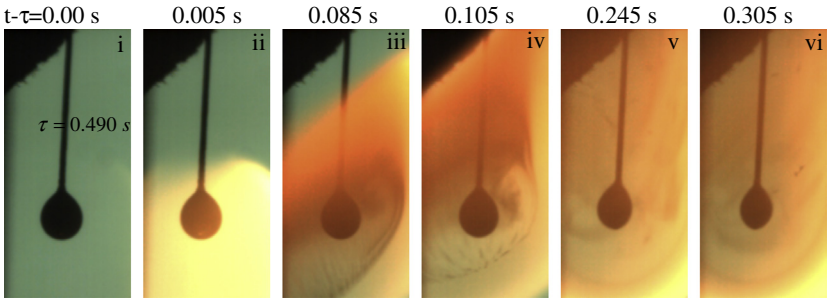

(a) Ignition **(i) Stage I** (b) Development, propagation and establishment of flame (c) Envelope flame **(iii-iv) Stage II**

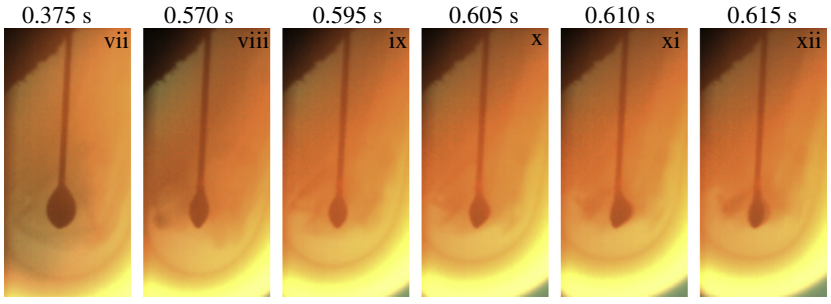

(d) Bubble pops up near the droplet's surface (e) Disruptive combustion

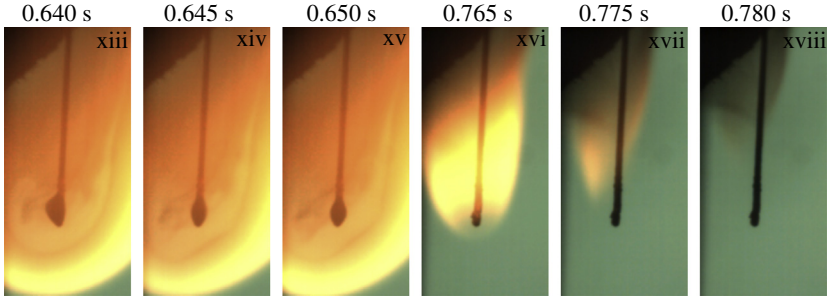

(f) Extinguish

(v-xviii) Stage III

(d)

Fig. 12 (*continued*)

of the combustion of hydrocarbon fuel, which was observed during the combustion of pure heptane and kerosene droplets and is in agreement with previous observations [25]. However, in *n*-Al/kerosene droplets combustion, this phenomenon was augmented, which indicates a substantial enhancement in the gasification of droplet. The disruptive burning behavior of *n*-Al/kerosene droplets was also different from that of *n*-Al/heptane droplets. The intensity and frequency of disruptions that occurred in kerosene-based nanofluid droplet was lower than the microexplosions that took place in *n*-Al/heptane droplets. This was most likely due to the higher boiling range of kerosene fuel (180–220 °C) compared with the boiling temperature of heptane fuel (98.3 °C). The Al NPs present at or nearer the droplet's surface may be heated more readily than the surrounding kerosene, as well as by absorption of the heat radiated from the flame following ignition, leading to a temperature in excess of that of the surrounding liquid. However, due to higher boiling point of base fuel, the NPs present inside the droplet were not able to achieve a temperature higher than the local boiling point and could not create HNSs deep within the inner core of the droplet. Consequently, the liquid fuel was gasified only at the droplet's surface and not inside the droplet. Therefore, these disruptions were not so much effective as the microexplosions that occurred in *n*-Al/heptane droplets. However, under a dilute loading rate, because of the low tendency of agglomeration, the particles had enough chances to escape from the droplet and burn via these disruptions. This is why nearly all of the NPs moved out of the droplet to burn in the flame. Therefore, almost no agglomerates (*i.e.*, residue) remained on the fiber, and an 'Al droplet flame' was not observed. Here, it is important to mention that the presence of residue is a key blocking factor for the practical use of metallized fuels which previously restricted the application of slurry fuels [1]. Further experimental studies are required to explore the elimination of large agglomerates of NPs in highly loaded nanofluid fuels droplet combustion and the underlying factors and mechanisms responsible for this phenomenon.

3.2.4. Average combustion rate of n-Al/kerosene droplets

As discussed in the previous section, the disruptions in *n*-Al/kerosene droplets were not so intense as the microexplosions that occurred during the combustion of *n*-Al/heptane droplets [14].

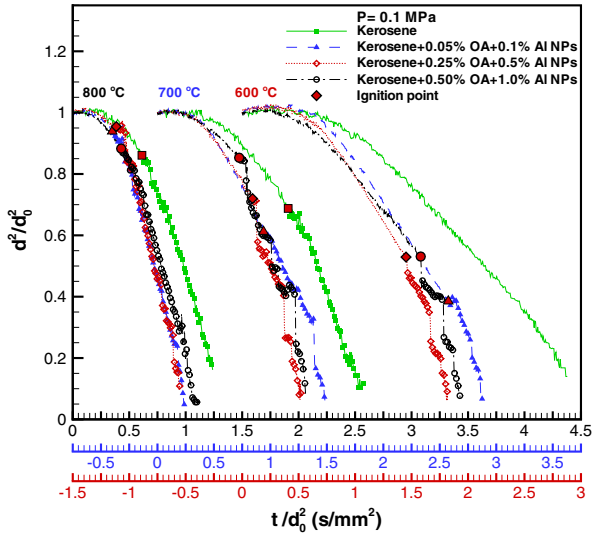

Fig. 13. Normalized temporal histories of *n*-Al/kerosene droplets' diameters squared containing dilute concentrations (0.1%, 0.5% and 1.0%) of Al NPs.

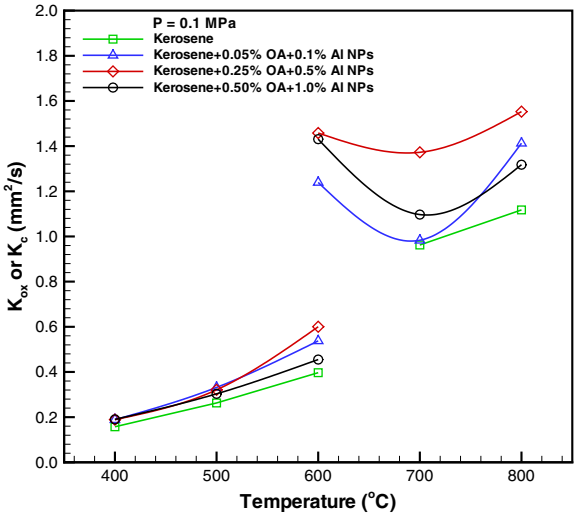

Fig. 14. Comparison of combustion rate constants between pure kerosene and *n*-Al/kerosene droplets containing dilute concentrations (0.1%, 0.5% and 1.0%) of Al NPs at various ambient temperatures.

Therefore, the approximate combustion rate constant could be calculated based on the droplet ignition diameter d_{ig} and burning time t_b. The least-squares method can be applied to the burning part of the experimental data to obtain the combustion rate of the kerosene-based nanofluid droplets. Thus, for the kerosene-based nanofluid droplets, the average combustion rate was defined as $K_b = {d_{ig}}^2/t_b$. Although after ignition, the droplet diameter squared did not vary linearly with time, the average combustion rate defined here is only a measure of the overall mass combustion rate, which provides the combined effect of NPs during the whole combustion process, *i.e.*, post-ignition enhanced gasification that causes vapor accumulation and disruptive burning.

3.2.4.1. Effect of ambient temperature on the average combustion rate. Figure 14 compares the oxidation and approximate combustion rate constants of kerosene-based nanofluid droplets containing dilute concentrations (0.1%, 0.5%, and 1.0%) of Al NPs with those of pure kerosene droplets under various ambient temperatures. The droplet oxidation rates were obtained from the linear part of the curves at low temperatures, where ignition/combustion was not occurred. The oxidation rates were obtained in order to distinguish the effects of combustion (or flame appearance) in *n*-Al/kerosene droplets that observed at relatively high temperatures. This figure clearly shows that the addition of dilute concentrations of Al NPs to kerosene enhanced the oxidation and combustion rates at all temperatures in the range 400–800 °C. The trend in the oxidation rate curves of the kerosene-based nanofluid fuel droplets is similar to those for pure kerosene, *i.e.*, the oxidation rate increased monotonically as the temperature increased from 400 to 600 °C. However, the combustion rate of kerosene-based nanofluid fuels increased substantially with temperature and in a different manner than pure kerosene. Probably, the oxidation rate was increased only due to enhanced thermal diffusion as a result of particle addition to droplet. The substantial increase in the combustion rate of *n*-Al/kerosene droplets was because of much faster heat transfer from the surrounding flame likely due to enhanced thermal diffusivity of the droplet as well as through radiative heat transfer from the flame. The high values of combustion rate at 600 °C, irrespective of NPs concentrations, were due to the ignition that occurred almost at the end of droplet lifetime, which resulted in a small burning time. However, from 700 to 800 °C, the burning rate constants of *n*-Al/kerosene droplets increased with increases in temperature similar to the pure kerosene droplets.

3.2.4.2. Effect of NP concentration on the average combustion rate. Figure 14 clearly indicates that the average combustion rate of the kerosene-based nanofluid droplets was also affected by the concentration of the NPs. As the NP concentration increased from 0.1% to 1.0%, the oxidation rates at relatively low ambient temperatures (400–600 °C) increased initially and then decreased. This reduced enhancement in the oxidation rate was most likely caused by the formation of NP agglomerates in the 1.0% Al NP suspension droplets, as discussed in the Section 3.1.1. At ambient temperatures of 600–800 °C, the combustion rate also increased with the NP concentration up to 0.5% and then decreased, becoming lower than the combustion rate of the 0.1% NP suspension at 800 °C but higher than the combustion rate of pure kerosene. The maximum increasing effect was also obtained with the 0.5% Al NP suspension at these temperatures. A possible explanation is that when the concentration of ligand-protected NPs increased beyond a critical value (0.5% in this case), more heat was transferred to the Al NPs rather than to liquid, thereby reducing the combustion rate enhancement.

4. Conclusions

We have experimentally investigated the effects of dilute concentrations of Al NPs on the autoignition and combustion behavior of kerosene-based nanofluid fuel droplets at various ambient temperatures. The aim of this work was to gain an improved understanding of the autoignition and combustion characteristics of such multi-component hydrocarbon-based nanofluid fuels. Similar to heptane-based nanofluid droplets [14], the autoignition delay time of kerosene-based nanofluid fuel droplets also decreased exponentially with increasing ambient temperature and can be expressed by the same Arrhenius functional form, $\tau = A\exp(D/T)$. The major results of this work can be summarized as follows.

(1) The addition of dilute (0.1%, 0.5% and 1.0%) concentrations of Al NPs lowered the minimum ignition temperature of kerosene droplets to 600 °C at which the pure kerosene droplet of same (1 mm) initial diameter was not ignited otherwise. These dilute concentrations of NPs also reduced the ignition delay time at 700–800 °C compared to pure kerosene.

(2) In contrast to pure and stabilized kerosene droplets, the *n*-Al/kerosene droplets exhibited disruptive burning behavior at all combustion temperatures and did not obey the classical d^2-law. However, with dilute loading of NPs, the intensity of these disruptions was low, and the least squares method could be applied to calculate the approximate combustion rate constant.
(3) The NPs were ejected from the droplets via these disruptions, and almost no residue or agglomerated NPs remained on the fiber, and consequently, no separate Al flame was observed. Probably, this is because of the low tendency of agglomeration under a dilute loading rate that almost all NPs escaped from the droplet and burn via these disruptions.
(4) The combustion rate of *n*-Al/kerosene droplets was substantially higher than the combustion rate of pure kerosene droplets. This enhancement in combustion rate was due to multiple-time droplet ruptures occurring in the nanofluid droplets at these temperatures.

Acknowledgment

This work was supported by the Midcareer Researcher Program through the NRF Grant funded by MEST (2010-0000353).

Appendix A. Supplementary material

Supplementary data associated with this article can be found, in the online version, at http://dx.doi.org/10.1016/j.combustflame.2014.08.018.

References

[1] P. Roy Choudhury, Prog. Energy Combust. Sci. 18 (1992) 409–427.
[2] B. Van Devener, S.L. Anderson, Energy Fuels 20 (2006) 1886–1894.
[3] B. Van Devener, J.P.L. Perez, J. Jankovich, S.L. Anderson, Energy Fuels 23 (2009) 6111–6120.
[4] H. Tyagi, P.E. Phelan, R. Prasher, R. Peck, T. Lee, J.R. Pacheco, P. Arentzen, Nano Lett. 8 (2008) 1410–1416.
[5] J.L. Sabourin, R.A. Yetter, B.W. Asay, J.M. Lloyd, V.E. Sanders, G.A. Risha, S.F. Son, Propellants, Explos., Pyrotech. 34 (2009) 385–393.
[6] C. Allen, G. Mittal, C.J. Sung, E. Toulson, T. Lee, Proc. Combust. Inst. 33 (2011) 3367–3374.
[7] M. Jones, C. Li, A. Afjeh, G. Peterson, Nanoscale Res. Lett. 6 (2011) 246.
[8] I. Javed, S.W. Baek, K. Waheed, G. Ali, S.O. Cho, Combust. Flame 160 (2013) 2955–2963.
[9] I. Javed, S.W. Baek, K. Waheed, Exp. Therm. Fluid Sci. 56 (2014) 33–44.
[10] I. Javed, S.W. Baek, K. Waheed, Combust. Flame 160 (2013) 170–183.
[11] J. Sabourin, D. Dabbs, R. Yetter, F. Dryer, I. Aksay, ACS Nano 3 (2009) 3945–3954.
[12] Y. Gan, L. Qiao, Combust. Flame 158 (2011) 354–368.
[13] Y. Gan, Y.S. Lim, L. Qiao, Combust. Flame 159 (2012) 1732–1740.
[14] I. Javed et al., Combust. Flame 162 (1) (2015) 191–206.
[15] T. Edwards, J. Propul. Power 19 (2003) 1089–1107.
[16] H. Ghassemi, S.W. Baek, Q.S. Khan, Combust. Sci. Technol. 178 (2006) 1031–1053.
[17] H. Ghassemi, S.W. Baek, Q.S. Khan, Combust. Sci. Technol. 178 (2006) 1669–1684.
[18] Q.S. Khan, S.W. Baek, H. Ghassemi, Combust. Sci. Technol. 179 (2007) 2437–2451.
[19] H. Ghassemi, S.W. Back, Q.S. Khan, 43rd Aerospace Sciences Meeting and Exhibit, 2005.
[20] C.K. Law, Combustion Physics, Cambridge University Press, 2006.
[21] S.R. Turns, An Introduction to Combustion: Concepts and Applications, McGraw-Hill Science, 2006.
[22] D.B. Spalding, Some Fundamentals of Combustion, Butterworth, London, 1955.
[23] M. Takei, T. Tsukamoto, T. Niioka, Combust. Flame 93 (1993) 149–156.
[24] S.K. Aggarwal, Prog. Energy Combust. Sci. 24 (1998) 565–600.
[25] H. Hara, S. Kumagai, Symp (Int) Combust 25 (1994) 423–430.